EXTENSIVE INVESTIGATIONS ON RADIAL CRACK FORMATION IN LABYRINTH SEALS OF AIRCRAFT ENGINES

L. Hühn[1], F. Rieger[1], F. Bleier[1], C. Schwitzke[1], H.-J. Bauer[1], T. Behnisch[2]
[1]Institute of Thermal Turbomachinery (ITS)
Karlsruhe Institute of Technology (KIT)
Kaiserstr. 12, 76131 Karlsruhe, Germany
[2]Institute of Lightweight Engineering and Polymer Technology (TUD)

Abstract

Labyrinth seals are due to their non-contact function and their thermal resistance the state of the art in sealing technology for thermal turbomachinery such as jet engines. The purpose of labyrinth seals is to adjust or minimize the leakage between rotor and stator. However, because of transient flight manoeuvres and the resulting mechanical and thermal loads on the components, contact between rotating and stationary parts cannot be ruled out. The aim of this study is to extend the basic understanding of the mechanisms of hot crack formation in the components of a labyrinth seal during the rubbing process. Previous investigations at the Institute of Thermal Turbomachinery have shown that the thermally induced stress caused in connection with the thermal change of the material properties can lead to formation of the cracks in the seal fin.
In order to get a deeper understanding of the complex crack initiation mechanisms, it is necessary to carry out fundamental experiments on simplified geometries. For this purpose, the stress conditions of a loaded labyrinth seal are applied to a cylindrical test specimen. It is fixed on both sides and subjected to thermo-cyclic load. To model a rubbing process of a labyrinth seal, the initial temperature of the cycle corresponds to the operating temperature of the rotor in a jet engine and the final temperature corresponds to the contact temperature during the rubbing process. The temperature change causes stress in the specimen due to the rigid mounting. In literature there are analytical considerations regarding the stress-strain curve in the seal fin and a possible pre-damage of the components by remaining tensile stress after the rubbing process. In this paper, these analytical approaches are compared with the test data. Also a residual tensile strength of the seal fin which is still to be tolerated is worked out depending on the temperature load. The stress reduction during heating is very significant and is considered in detail. Due to the high mechanical and thermal loads, the stress reduction is superimposed by relaxation and plastic deformation. For a separate consideration of these basic effects, FE simulations are carried out.
The main findings are that stress and strain in the component depends on both the initial and the final temperature of the specimen. The final rubbing temperature mainly influences the remaining tensile stress. With the thus calculated remaining strength of the seal fin a probable crack formation could be determined. The evaluation of this data contributes significantly to the understanding of hot crack formation in labyrinth seal fins and is therefore the basis for the optimization of the sealing system with regard to robustness against rubbing processes.

Keywords

Labyrinth seal fin rubbing; radial crack formation; cyclic temperature load; experimental investigation; jet engines

1. INTRODUCTION

The Flightpath 2050 imposes high demands on the aircraft engine of the future. Reducing emissions and increasing efficiency are the main requirements [1]. Therefore, component efficiencies should be improved. Reducing the clearance in the flow paths and secondary air system is an effective method to minimize the parasitic airflow leakage [2]. The most frequently used sealing system in the secondary air system is the labyrinth seal. Reasons are their simple design, reliability and thermal resistance [3].
The aim of labyrinth seals is to control and minimize the leakage between rotor and stator. They are non-contacting seals, but due to mechanical and thermal expansion of components, caused for example by transient flight manoeuvres, contact between rotor and stator cannot be ruled out. In order to increase the efficiency of the labyrinth seal, the clearance between the rotor and stator should be as small as possible [4, 2]. Thus, the risk of contact increases. Therefore, the seal has to tolerate these rubbing events, which returns in high demands on the used seal fin materials and a abrasive design of the stator.
According to Rossmann [5], the most frequent and fatal consequence are radial cracks in the labyrinth seal fin which may lead to serious damages. Therefore, the main objective is to understand this crack initiation.

doi:10.25967/480120

Ghasripoor et al. [6], Munz et al. [7] and Pychynski et al. [8] investigated numerically and experimentally the rubbing behaviour between labyrinth seal fins and the stator part. It has been shown that material, labyrinth geometry, and rubbing conditions (friction velocity, incursion rate, and incursion depth) have a large influence on the resulting contact forces and temperatures during rubbing. Similar to Munz et al. [7], Inconel 718+ is investigated as rotor material in this paper.
Pychynski et al. [9] discuss analytically and numerically the stress in the rotor resulting from rubbing processes and rotation. It has been proving that the high local temperature in the contact surface during rubbing most likely is the reason for radial cracks in the seal fin. The local temperature increase causes thermally induced remaining tensile stress in the component. This stress can lead to crack initiation in connection with additional tensile stress due to centrifugal forces and deteriorated material properties at high temperatures. This correlation will be explained in more detail further on.
The thermal load on the seal fin material can be modelled using thermomechanical fatigue tests (TMF). The production of the super-alloy used is decisive for the resulting load in the component. Fahrmann et al. [10] investigated an alloy similar to that presented in this paper. Depending on the cooling rate from the prior annealing temperature to the test temperature, different primary γ' and secondary γ' are produced. These have an influence on the material properties at higher temperatures.
Affeldt et al. [11] and Ahmed et al. [12] investigated the material behaviour of Haynes 230 under cyclical temperature loading and combined cyclical strain and temperature loading. Haynes 230 is also a super-stress

alloy which has similar properties to those studied in this paper. If the temperature reaches a certain limit, the materials begin to creep plastically. Cyclic hardening or softening is the result. The material therefore shows hysteresis behaviour under cyclic load. Affeldt et al. [11] also observed a correlation of cyclic deformation and crack growth caused by high-temperature oxidation at the crack tips. However, the crack initiation and the connection of the rubbing with the TMF tests has not yet been investigated.

The objective of this paper is to extend the understanding of the crack initiation. The first part of this paper deals with the experimental validation of the analytical approaches in Pychynski et al. [9]. For this purpose, TMF tests were carried out on a simplified geometry. The current study aims to determine the relationship between temperature load and the resulting stress and strain in the specimen. A gauge for the determination of the crack probability should be found. In addition, the physical effects during the heating of the specimen are investigated in detail. Due to the high mechanical and thermal loads, the stress reduction is superimposed by relaxation and plastic deformation. For a separate consideration of these basic effects, FE simulations are performed.
The evaluation of this data contributes significantly to the understanding of hot crack formation in labyrinth seal fins and is thus the basis for the optimization of the sealing system with regard to robustness against rubbing processes.

2. EXPERIMENTAL INVESTIGATIONS

The goal of the thermomechanical fatigue tests is to represent the real temperature load condition of a labyrinth seal fin in a jet engine. Therefore, tests were carried out with different temperature boundary conditions.

In order to explain the connection between TMF tests and the loaded seal fin, the rubbing process is first explained schematically. A sketch of the rubbing labyrinth seal is shown in FIGURE 1.

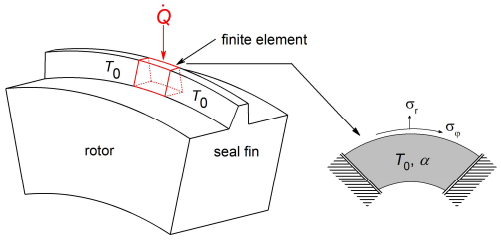

FIGURE 1. Left side: Finite element of the seal fin, Right side: Resulting simplified geometry

The local rubbing contact at the red marked finite element is symbolized by the heat flux $\dot{Q}$. This heat supply leads to a local temperature increase of the seal fin. The contact forces are negligibly small and are therefore not taken into account. The material outside the contact has the significantly colder operating temperature of the rotor. This material fixes the finite element which expands due to the local heating and thus introducing thermal compressive stress. If the stress exceeds the yield strength, its leads to residual tensile stress when the component cools down again.
The simplified geometry with the fixed mounting in tangential direction is shown in FIGURE 1 on the right side. The resulting radial σ_r and axial σ_ax stress caused by the rotation of the component are also marked. As described in [9] the internal tensile stress which occurs during cooling is much higher and can induces radial cracks in the seal fin.
According to [9] the load on the seal fin can be modelled as a test specimen fixed on both sides and loaded thermocyclic. The initial temperature T_0 of the cycle corresponds to the operating temperature of the rotor in a jet engine and the final temperature T_E corresponds to the contact temperature during a typical rubbing process. The test setup is described further.

2.1. Thermomechanical fatigue tests

The material used is the nickel based super-alloy Inconel 718+. The material properties are mainly determined by the primary γ' and the secondary γ' [10,13]. These lead to a good temperature and corrosion resistance. Even at high temperatures, the yield strength and the Young's Modulus are higher than in other materials.
In FIGURE 2 the test setup is depicted.

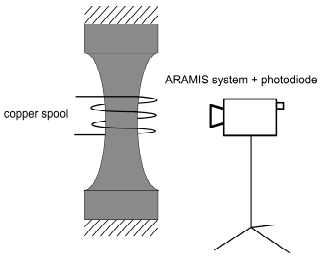

FIGURE 2. Schematic drawing of the test rig structure

In the experiment, axial mounts of a servo-hydraulic testing machine realize the fixed mounting of the test specimen. The heating is realized inductive by a copper spool. Due to the high test temperatures, temperature and strain measurements are performed optically. The forces are measured at the fixed mounting. For further information on the test setup, please refer to Höhn [14].

The cyclical temperature load is shown in FIGURE 3.

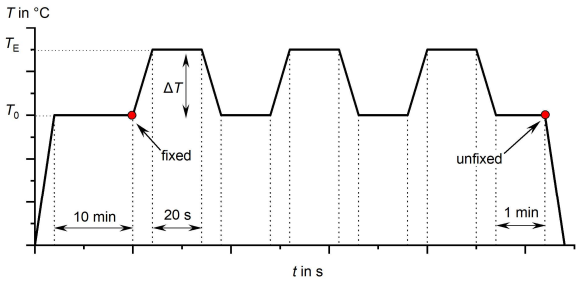

FIGURE 3. Diagram of the cyclical temperature load

The investigated initial and final temperatures are listed in TAB. 1.

T_E in °C	T_0 300°C	T_0 400°C	T_0 500°C	T_0 600°C
500		X		
600	X	X	X	
700	X	X	X	X
800	X	X	X	X
900	X		X	X
1000	X			X

TAB. 1 Performed experiments

In the experiment, the specimen is first heated to the initial temperature T_0. This temperature is then maintained for 10 minutes to achieve a constant temperature across the entire geometry. To ensure that no stress is applied during the heating phase, the testing machine fixes the specimen after this holding phase. The next step is to heat up the specimen evenly to the final temperature T_E and hold the temperature for 20 seconds. It is then cooled down to T_0 by ambient air. After one heating and cooling phase one cycle is complete. As depicted in FIGURE 3, three cycles are carried out during each test programme. A hysteresis stress-strain behaviour is expected from the cyclic load.

2.2. Results and Discussion

In order to gain a better understanding of the presented experimental results, the analytical considerations of [9] will be summarized briefly.

To show the cyclic hysteresis behaviour of the material, the nominal stress is plotted over the total strain in FIGURE 4. The expected stress-strain behaviour is modified to the considerations of Pychynski et al. [9]. Compared to his investigations, the total and not the thermal strain is depicted here. He assumed, that the yield strength $R_{p0,2}$ decreases with increasing temperature. Therefore, an ideal elastic-plastic behaviour without hardening is explained.

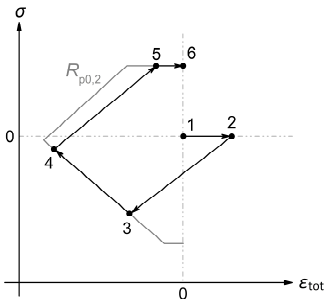

FIGURE 4. Modified stress-strain curve according to Pychynski et al. [9]

The stress-strain curve of one cycle is composed of the following phases (see also FIGURE 3):

- **Phase 1** (Point 1 to 2)
  Heating up to T_0: Stress-free, thermal expansion of the not fixed specimen due to heating to T_0.

- **Phase 2** (Point 2 to 4)
  Heating up to T_E: Compressive stress in the specimen. If the stress exceeds the yield strength (Point 3), plastic deformation and stress reduction along the yield strength curve occur as function of T, shrinkage of the specimen due to the compressive stress.

- **Phase 3** (Point 4 to 6)
  Cooling down to T_0: Tensile stress occurs due to the fixation. If the yield strength is exceeded again (Point 5), plastic effects also occur during cooling.

The analytically explained behaviour corresponds to the results of the experiments. In FIGURE 5 an example of the nominal stress above the total strain for the tests: $T_0 = 400°C$, $T_E = 600°C$ and $T_0 = 400°C$, $T_E = 700°C$ is shown.

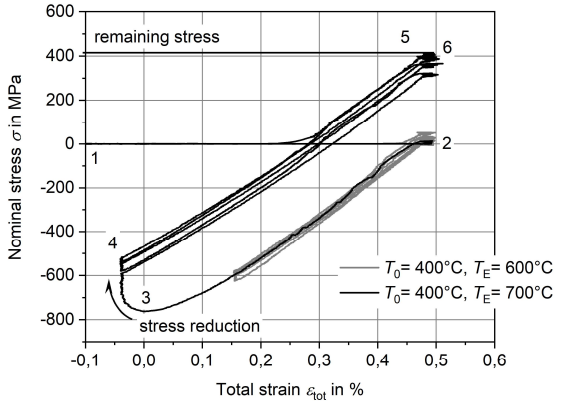

FIGURE 5. Nominal Stress-Strain Diagram for $T_0 = 400°C$, $T_E = 600°C$ and $T_0 = 400°C$, $T_E = 700°C$

The total strain ϵ_{tot} is calculated from the measured positive strain of the specimen during heating to T_0 (Phase 1) and the thermally induced strain ϵ_{th}:

(1) $\epsilon_{tot} = \epsilon_{th} + \epsilon_{exp} = \alpha\, \Delta T\ + \epsilon_{exp}.$

The coefficient α is the thermal expansion coefficient depending on the temperature. The shape of the hysteresis loop changes with the initial and final temperature. The test with $T_0 = 400°C$ and $T_E = 600°C$ shows a purely elastic behaviour (without Point 3 and Point 5). If the area in the hysteresis loop is constant over the cycles, plastic stress must be assumed.

The black curve in FIGURE 5 shows stress for the test with $T_0 = 400°C$ and $T_E = 700°C$. The compressive stress is reduced during the heating process by plastic deformation and relaxation. Due to the relevance for crack formation, the stress reduction processes will be considered separately later on.
Because of the fixed mounting, remaining tensile stress σ_{rem} is generated in the specimen as soon as plastic effects occur during heating. To explain the consequences of this remaining tensile stress, the stress conditions after a rubbing process are shown in FIGURE 6.

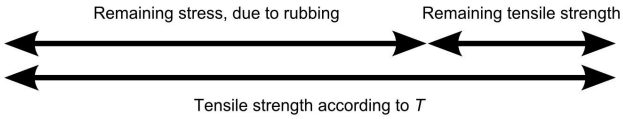

FIGURE 6. Stress conditions after a rubbing process

With the three depicted parameters, the crack initiation could be described. After a rubbing process there is a remaining tensile stress σ_{rem} in the seal fin. Additionally, the tensile strength is reduced due to the high operating temperature of the rotor in a jet engine.
The difference between the two is the remaining tensile strength which can still be tolerated by the seal fin after rubbing. A crack can occur if the remaining tensile strength is lower than tensile stress due to centrifugal forces.
All parameters involved in the crack initiation process are now examined in more detail.

Remaining stress

In FIGURE 7 the tensile stress after cool-down as a function of the initial temperature T_0 and the final temperature T_E is depicted.

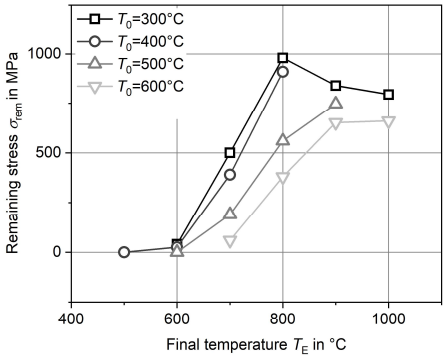

FIGURE 7. Remaining tensile stress σ_{rem} as a function of the initial temperature T_0 and ΔT

It is demonstrated that there are tests in which no remaining tensile stress occurs and above a certain temperature difference the remaining tensile stress is constant or is decreasing again. If the remaining tensile stress decreases at high temperatures, the stress in the specimen exceed sthe yield strength during the cool down phase. Due to material damage, this state should not be reached. It can be summarized that the remaining stress increases with the final temperature (= rubbing temperature).

Remaining tensile strength

To calculate the remaining tensile strength of the seal fin, it is necessary to refer to tensile strength data from literature. FIGURE 8 shows the tensile strength of Inconel 718+ over temperature.

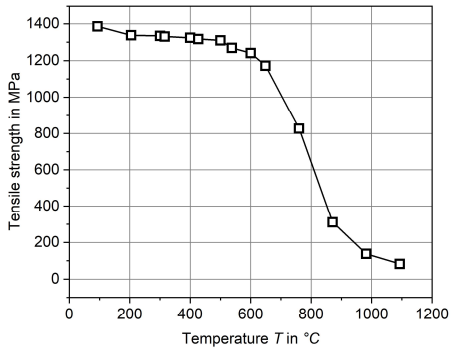

FIGURE 8. Tensile strength of Inconel 718+ over the temperature modified according to [13]

The diagram shows a barely decreasing tensile strength up to temperatures of $600°C$. The remaining strength as a function of delta T_0 and T_E is shown in FIGURE 9.

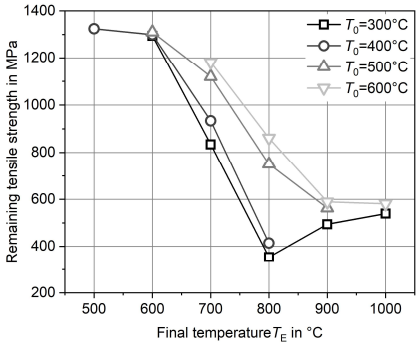

FIGURE 9. Remaining strength as a function of the initial temperature T_0 and the final temperature T_E

The remaining tensile strength σ_rem decreases with increasing final temperature. Only at high temperatures over $800°\mathrm{C}$ the remaining tensile strength rises again. The change due to plastic pre-damage as for example a hardening of the specimen is not taken into account yet. This may be a reason for the increasing strength of the $T_0 = 300°C$ curve in FIGURE 9. In the worst scenario, additional tensile stress of less than $400\ \mathrm{MPa}$ is sufficient to initiate a crack. These can be achieved by centrifugal forces.
The reduction of the final temperature is very effective in increasing the residual tensile strength. As the jet engine's operating temperature T_0 cannot be influenced without major efficiency losses, T_E can only be reduced by reducing the heat input during the rubbing process.

It could be shown that if the material behaviour at high temperatures and the residual tensile stress after a rubbing event are known, critical operating conditions for a labyrinth seal can be identified. The stress reduction during heating is responsible for the formation of the remaining tensile stress. This relationship is now being examined in more detail.

FIGURE 10 shows the remaining tensile stress σ_rem measured experimentally over the stress reduction σ_{red} in the first cycle.

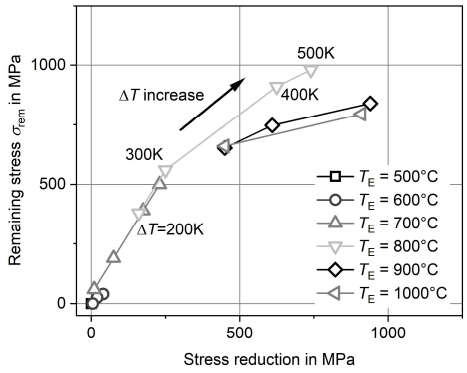

FIGURE 10. Remaining tensile stress over the pressure reduction in one cycle. The lines indicate different final temperatures T_E. The label of the curve with $T_\mathrm{E} = 800°\mathrm{C}$ corresponds to the temperature difference $\Delta T = T_\mathrm{E} - T_0$

The diagram illustrates that the remaining tensile stress depends on the reduction of compressive stress in the first cycle. The temperature differences ΔT are shown as an example for the curve of $T_\mathrm{E} = 800°\mathrm{C}$. The higher the temperature difference, the more pressure is reduced, respectively the more residual tensile stress remains in the specimen. At final temperatures above $900°\mathrm{C}$, the remaining tensile stress σ_rem is lower than expected from the reduction of compressive stress. Reasons could be hardening effects of the material structure or the reaching of the yield strength during cooling phase. Further investigations should be carried out. However, FIGURE 10 demonstrates that the tensile stress remaining in the specimen can be determined by the stress reduction in the first cycle.

A precise knowledge of the pressure reduction processes is therefore of great importance. The total pressure reduction per cycle can be divided into the stress reduction during heating and the reduction during the holding phase (see FIGURE 3). FIGURE 11 shows the division of the pressure reduction σ_{red} and the remaining tensile stress over the final temperature depending on the start temperature ($T_0 = 400°\mathrm{C}$ and $T_0 = 600°\mathrm{C}$).

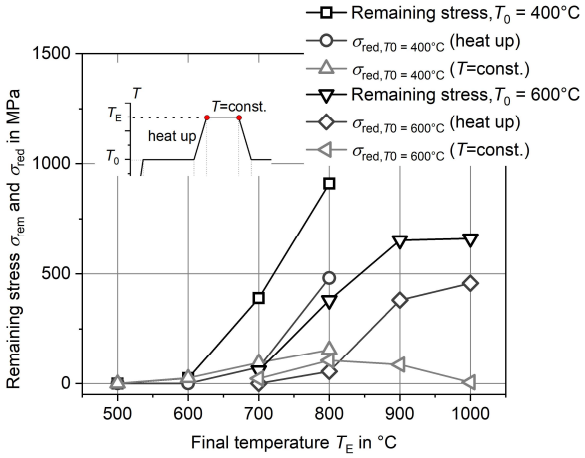

FIGURE 11. Remaining tensile stress σ_rem and pressure reduction σ_{red} over final temperatures T_E for $T_0 = 400°\mathrm{C}$ and $T_0 = 600°\mathrm{C}$

For a better overview, only stress curves for initial temperatures $T_0 = 400°\mathrm{C}$ and $T_0 = 600°\mathrm{C}$ are shown. At lower final temperatures, more stress is reduced in the holding phase compared to the heating phase. This is done by relaxation at constant temperature and constant elongation. Above $800°\mathrm{C}$ final temperature, the compressive stress is mainly reduced during the heating phase. This can be explained by the high temperatures and therefore the lower yield strength leading to strong plastic deformation in the specimen. At $T_\mathrm{E} = 1000°\mathrm{C}$ the complete compressive stress is reduced during heating. Relaxation during the holding phase therefore does not take place.

Relaxation and plastic effect overlap during stress reduction. Relaxation occurs from a temperature of $0.4T_\mathrm{melt}$ [15]. With a melting temperature $T_\mathrm{melt} = 1336°\mathrm{C}$ of Inconel 718+, relaxation starts at $370°\mathrm{C}$ [13].In order to consider these separately, further numerical investigations are required.

3. NUMERICAL INVESTIGATION

In order to be able to examine the stress reduction processes more detailed, FE simulations of the simplified specimen are made. The FE simulations are carried out with the modelling software COMSOL Multiphysics®. To obtain only the plastic part of the stress reduction during heating, relaxation in the component is not modelled.

3.1. Numerical setup

A 15mm long cylinder with a diameter of 6mm is used as geometry according to the specimen from the tests. Only the heating process from T_0 to T_E is simulated.
The temperature-dependent material model for Inconel 718 from the existing material database is used. In addition, thermal expansion and plasticity are selected. The strain reference temperature depends on the initial temperature T_0 in order to represent the stress-free expansion when heating up to T_0. Large plastic deformations are expected. If the Mises equivalent stress exceeds the yield strength, plastic deformation occurs. For this purpose, a temperature-dependent yield strength and the isotropic tangent module for the linear isotropic hardening model must also be implemented in the material behaviour. The isotropic tangent module is calculated from the material properties to 2500MPa.

The specimen is fixed on both circular surfaces of the cylinder. The initial temperature is set homogeneously as T_0 in the complete specimen. The heating process to T_E is specified as a function of the simulated time: $T(t) = T_0 + \frac{T_\text{E}-T_0}{2} + \frac{T_\text{E}-T_0}{2} cos(\frac{t}{t_\text{sim}}\pi + \pi)$. This corresponds to the heating up in the experiment and enables a homogeneous temperature distribution at the end of the simulation. It is calculated time-dependently in order to calculate the plastic and temperature-dependent material behaviour correctly. t_sim is the simulated time and is 10s.

3.2. Results and Discussion

In FIGURE 12 the stress field of the mises equivalent stress at the surface of the specimen for the simulation with $T_0 = 400°\text{C}$ and $T_\text{E} = 600°\text{C}$ is shown.

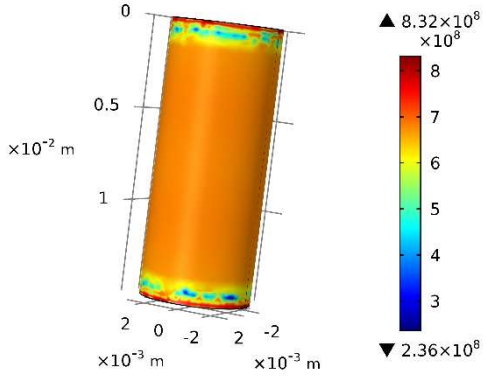

FIGURE 12. Mises equivalent stress in Pa at the surface of the specimen for the simulation with $T_0 = 400°\text{C}$ and $T_\text{E} = 600°\text{C}$

The colouring corresponds to the Mises equivalent stress in Pa. After $10s$ simulated time a homogeneous stress over the specimen occurs. The stress discontinuities at the mounting are due to singularities of the simulation. In order to not take into account the influence of this discontinuity on the stress in the specimen, the stress is evaluated in the centre of the specimen in the following.

The axial stress σ_ax generation during the simulation time for the tests $T_0 = 400°\text{C}, T_\text{E} = 600°\text{C}$ and $T_0 = 400°\text{C}, T_\text{E} = 800°\text{C}$ is now considered. Therefore, σ_ax is shown over the temperature rise of the specimen in FIGURE 13.

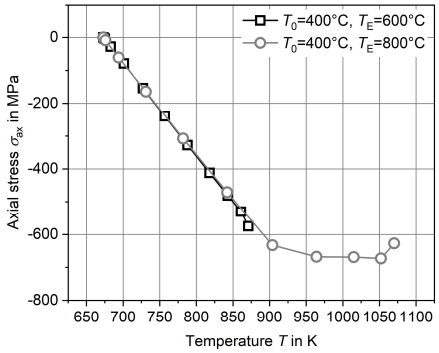

FIGURE 13. Axial stress σ_ax generation for the tests with $T_0 = 400°\text{C}, T_\text{E} = 600°\text{C}$ and $T_0 = 400°\text{C}, T_\text{E} = 800°\text{C}$ over the temperature in the specimen

The data points correspond to the simulated time $t_\text{sim} = 0 - 10\text{s}$. First, the stress increase linearly. At a temperature of 900K plastic effects occur.

In FIGURE 14 the calculated axial stress is compared with the measured stress at the end of the heating process.

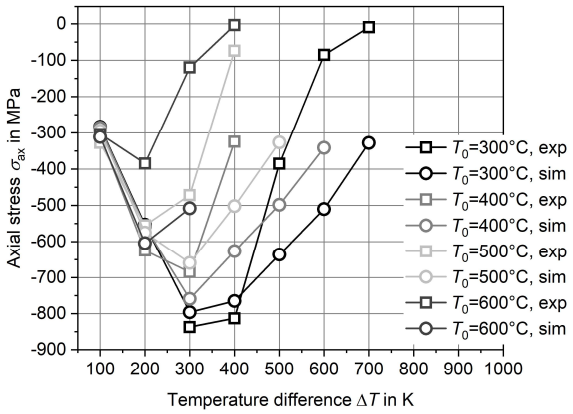

FIGURE 14. Measured and simulated axial stress σ_ax plotted over the temperature difference ΔT for different initial temperatures T_0

At low temperature difference (up to $\Delta T = 200\text{K}$) the simulated and measured axial stress correspond well. This means that relaxation effects plays a subordinate role at low temperatures. With increasing temperature differences the deviation of the stress increase.

For a more detailed discussion, the difference $\Delta\sigma_\text{ax} =$

$\sigma_{\mathrm{ax,sim}} - \sigma_{\mathrm{ax,exp}}$ between the simulated and measured axial stress are shown in FIGURE 15. Since the model does not consider relaxation, this difference is a measure of the proportion of relaxation in stress reduction during heating up.

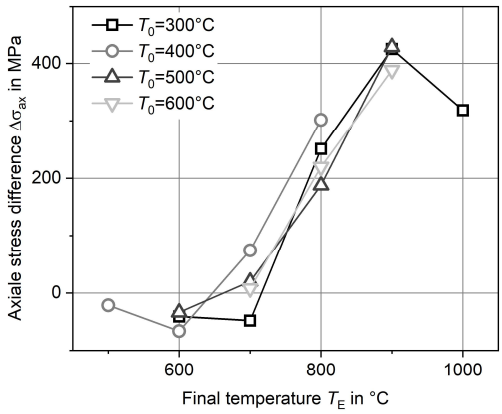

FIGURE 15. $\Delta\sigma_{\mathrm{ax}}$ over the temperature difference for different T_0

At low temperature differences (up to $\Delta T = 100\mathrm{K}$) the simulated stress is below the measured stress. This is based on the linear isotropic hardening model. From $\Delta T = 200\mathrm{K}$ the simulated compressive stress is always higher than those determined experimentally. The reason for this is the stress reduction due to relaxation effects which are not taken into account in the simulation model. Relaxation is a temperature dependent process. The higher the temperatures in the component, the faster stress is reduced due to relaxation. This explains the increasing deviation of the measured and simulated axial stress with increasing ΔT.

With the help of the FE simulations, the stress reduction during heating could be investigated in more detail. With this knowledge, the remaining tensile stress in the seal fin relevant for crack formation can be predicted better.

4. CONCLUSION

The aim of this paper was to investigate the processes of hot crack initiation in labyrinth seal fins. Firstly, a possible test procedure for a simplified modelling of the loaded seal fin was presented.
Secondly, analytical considerations from Pychynski et al. [9] were verified with the experimental data. It could be shown that depending on the temperature load the thermally induced stress leads to the resulting remaining tensile stress in the component. In combination with the reduced yield and breaking strength at the high operating temperatures of the jet engine, less than $400\ \mathrm{MPa}$ additional tensile stress may be sufficient to initiate a crack in the seal fin. This tensile stress can be caused by centrifugal forces. Therefore, it could be shown that with the help of the thermomechanical fatigue test and data from the literature a range of the most probable crack formation can be identified.

Furthermore, the compressive stress reduced during the heating and holding phases could be identified as the reason for the remaining tensile stress. A good knowledge of the pressure reduction processes should be provided. In order to investigate the pressure reduction processes more closely, additional FE simulations were presented. Only a plastic material model was implemented in the model. This allows a separate consideration of the stress reduction through plastic deformation without relaxation effects. At low final temperatures, the experimentally measured and simulated axial stress are well matched. This means that relaxation effects play a subordinate role at low temperatures. Stress reduction by relaxation increases with increasing temperature. With this knowledge, the remaining tensile stress in the seal fin relevant for crack formation can be better predicted.

5. NOMENCLATURE

symbol	unit	description
Shortcuts		
FE		Finite Element
TMF		Thermomechanical fatigue
Latin		
E	GPa	Young's Modulus
L	m	length
$\dot{Q}$	kg·m^2·s^{-3}	heat flux
$R_{p0,2}$	MPa	yield strength
T	°C, K	temperature
t	s	time
ΔT	K	temperature difference
Greek		
α	-	thermal expansion coefficient
ε	-	elongation
σ	MPa	stress
Subscripts		
0		initial
ax		axial
E		final
exp		experimental
melt		melting
r		radial
red		reduction
rem		remaining
sim		simulated
th		thermal
tot		total
φ		tangential

ACKNOWLEDGEMENT

The authors acknowledge the support from the European Commission through the FP7 E-BREAK project under Grant Agreement No. 314366.

References

[1] Darecki M. and others. *Flightpath 2050: Europe's vision for aviation ; maintaining global leadership and serving society's needs ; report of the High-Level Group on Aviation Research*. Publ. Off. of the Europ. Union, Luxembourg (2011).

[2] Schramm, V., Willenborg, K., Kim, S., and Wittig, S. “Influence of a Honeycomb Facing on the Flow Through a Stepped Labyrinth Seal.” *ASME Turbo Expo 2000: Power for Land, Sea, and Air* Vol. 2000: pp. V003T01A092. DOI 10.1115/2000-GT-0291.

[3] Chupp, R. E., Hendricks, R. C., Lattime, S. B., and Steinetz, B. M. “Sealing in Turbomachinery.” *Journal of Propulsion and Power* Vol. 22 No. 2 (2006): pp. 313–349. DOI 10.2514/1.17778.

[4] Braun, E., Dullenkopf, K., and Bauer, H.-J. “Optimization of labyrinth seal performance combining experimental, numerical and data mining methods.”. *Proceedings of the ASME Turbo Expo Turbine Technical Conference and Exposition, GT 2012; Copenhagen; Denmark; 11 June 2012 - 15 June 2012*: pp. 1847–1854. DOI 10.1115/GT2012-68077.

[5] Rossmann, A. *Die Sicherheit von Turbo-Flugtriebwerken - Reibverschleiß, Anstreifen und Spalthaltung, Labyrinthe: Band 2*. Turbo Consult, Karlsfeld (2001).

[6] Ghasripoor, F., Turnquist, N. A., Kowalczyk, M., and Couture, B. “Wear Prediction of Strip Seals Through Conductance.”. *ASME Turbo Expo 2004: Power for Land, Sea, and Air*: pp. 331–337. Vienna, Austria, June 14–17, 2004. DOI 10.1115/GT2004-53297.

[7] Munz, O., Schwitzke, B., Bauer, H.-J., Welzenbach, S., Fischer, T., and Ulan kyzy, S. “Modelling the Rubbing Process in Labyrinth Seals.”. *Proceedings of GPPS Forum 18, Zurich, CH, January 10-12, 2018*: pp. GPPS-2018-0038/ 1-9.

[8] Pychynski, T., Höfler, C., and Bauer, H.-J. “Experimental Study on the Friction Contact Between a Labyrinth Seal Fin and a Honeycomb Stator.” *Journal of Engineering for Gas Turbines and Power* Vol. 138 No. 6 (2016): pp. 062501/1-9. DOI 10.1115/1.4031791.

[9] Pychynski, T., Dullenkopf, K., and Bauer, H.-J. “Theoretical study on the origin of radial cracks in labyrinth seal fins due to rubbing.”. *Proceedings of the ASME Turbo Expo ASME Turbo Expo 2013: Turbine Technical Conference and Exposition, GT 2013; San Antonio, Tx; United States; 3 June 2013 through 7 June 2013*: p. GT2013-94834. DOI 10.1115/GT2013-94834.

[10] Fahrmann, M. and Suzuki, A. “Effect of Cooling Rate on Gleeble Hot Ductility of UDIMET Alloy 720 Billet: TMS (The Minerals, Metals & Materials Society).” (2008).

[11] Affeldt, E. E. and Cerdan de la Cruz, L. “Thermo-mechanical fatigue of a wrought nickel based alloy.” *Materials at High Temperatures* Vol. 30 No. 1 (2014): pp. 69–76. DOI 10.3184/096034013X13638694650058.

[12] Ahmed, R., Barrett, Paul R., Menon, M., and Hassan, T. “Thermo-mechanical low-cycle fatigue-creep of Haynes 230.” *International Journal of Solids and Structures* 126-127 (2017): pp. 90–104. DOI 10.1016/j.ijsolstr.2017.07.033.

[13] Special Metals Corporation. “INCONEL aloy 718: Publication Number SMC-045.”, 2007. URL http://www.specialmetals.com/assets/smc/documents/inconel_alloy_718.pdf.

[14] Höhn, C. “Methodenentwicklung zur Untersuchung des mechanischen Verhaltens von Inconel-718+ bei zyklischer thermischer Belastung.” Studienarbeit. Technische Universität Dresden, Dresden.

[15] Hornbogen, E. and Warlimont, H. *Metalle: Struktur und Eigenschaften der Metalle und Legierungen*. Springer Vieweg, Berlin, Heidelberg (2015).